HAL open science

Sensivity-based shape optimization of a rigid tramway low-height noise barrier

Alexandre Jolibois, Denis Duhamel, Victor W. Sparrow, Jérôme Defrance, Philippe Jean

To cite this version:

Alexandre Jolibois, Denis Duhamel, Victor W. Sparrow, Jérôme Defrance, Philippe Jean. Sensivity-based shape optimization of a rigid tramway low-height noise barrier. Internoise 2013, Sep 2013, Innsbruck, Austria. pp.726. hal-00869855

HAL Id: hal-00869855

https://hal.science/hal-00869855v1

Submitted on 4 Oct 2013

HAL is a multi-disciplinary open access archive for the deposit and dissemination of scientific research documents, whether they are published or not. The documents may come from teaching and research institutions in France or abroad, or from public or private research centers.

L'archive ouverte pluridisciplinaire **HAL**, est destinée au dépôt et à la diffusion de documents scientifiques de niveau recherche, publiés ou non, émanant des établissements d'enseignement et de recherche français ou étrangers, des laboratoires publics ou privés.

inter noise
2013 | INNSBRUCK | AUSTRIA
15.-18. SEPTEMBER 2013
NOISE CONTROL FOR QUALITY OF LIFE

Sensitivity-based shape optimization of a rigid tramway low-height noise barrier

Alexandre Jolibois[1], Denis Duhamel[2], Victor W. Sparrow[3], Jérôme Defrance[4] and Philippe Jean[5]

[1,2] Université Paris-Est, Laboratoire Navier, ENPC-IFSTTAR-CNRS, UMR 8205, Ecole des Ponts ParisTech
6 & 8 avenue Blaise Pascal, Champs-sur-Marne, 77455 Marne La Vallée Cedex 2, France
[3] Graduate Program in Acoustics, The Pennsylvania State University
201 Applied Science Building, University Park, 16802, USA
[4,5] Université Paris-Est, Centre Scientifique et Technique du Bâtiment
24, rue Joseph Fourier, 38400 Saint Martin d'Hères, France

ABSTRACT

An urban low-height barrier meant to attenuate tramway noise for nearby walking pedestrians or cyclists is considered. The efficiency of this type of device is known to depend on the shape of the cross section and the acoustic properties of the surface treatment. Some sort of absorptive material is often required to enhance the performance by preventing the multi-reflection phenomenon, however such materials can be costly compared to acoustically rigid materials such as concrete. In this study, a rigid barrier is assumed but its shape is optimized using a sensitivity-based shape optimization algorithm coupled to the two dimensional BEM. The shape is here described in a very general fashion by mesh nodes coordinates, which can involve a large number of variables. Sensitivities with respect to all coordinates are calculated efficiently using the adjoint state approach, without significant increase of computation time. Numerical results show that optimized shapes tend to be quite irregular but provide a significant improvement compared to simpler shapes, especially in the mid and high frequency range. Intensity calculations seem to suggest that this improvement is due to scattering of the incident acoustic energy in the upwards direction, therefore reducing the diffracted energy which reaches the shadow zone. Extra calculations show that the benefit of the optimized shapes can still be significant even in more realistic situations.
Keywords: Tramway, Barrier, Optimization

1. INTRODUCTION

After several decades of research and commercial development, noise barriers have become a very common noise control tool especially close to highways. However, there is an increasing concern to reduce

[1]alexandre.jolibois@enpc.fr
[2]denis.duhamel@enpc.fr
[3]vws1@psu.edu
[4]jerome.defrance@cstb.fr
[5]philippe.jean@cstb.fr

noise exposure in urban areas as well since noise is considered to be one of the most important nuisances in cities. In an urban environment, noise sources - cars, guided transportation tracks - and receivers - cyclists, pedestrians - are very close together, and of course building a wall 2 or 3 meters high along streets or tramway tracks is not a option that could be easily accepted by communities. Hence, the possibility of using a low height protection directly between the source and the receiver started to gain interest [1–7]. Because the distances between sources, other reflectors and a potential barrier is so small, the device shape and surface treatment are expected to have a stronger effect than in the highway case. It has been shown for instance that optimization of the surface treatment can yield a significant improvement of low-height barriers performance, especially when an absorbing treatment is present close to the source [4, 6, 7]. However, absorbing materials can be expensive or even be environmentally hazardous if not packaged properly, whereas acoustically rigid materials (such as concrete) are cheaper and easier to handle.

In this paper we hence consider a rigid low-height (maximum one meter high) barrier and we allow its shape to be optimized by a sensitivity-based iterative optimization method. The method is applied to a tramway low-height barrier, since this means of transportation has been rapidly developing in urban environments. Besides, Pallas et al. [8] measured that most of the noise emitted by a modern tramway comes from the rail track and the *bogie* (undercarriage structure) areas, which are close to the ground, and therefore a low height barrier would be likely to mitigate these sources effectively.

The attenuation provided by the barrier and its sensitivity (or gradient) with respect to shape changes are calculated efficiently using the boundary element method (BEM) and the adjoint state approach [9–11]. With this method, the sensitivity is expressed as a post-treatment of the BEM and therefore its calculation does not require coding a new solver. Moreover, a great number of variables can be used without significant increase of computation time, which makes it possible to describe the shape in a very general manner by the mesh nodes coordinates. Finally, the choice of a gradient-based optimization method as opposed to a stochastic approach has been made to take advantage of the sensitivity information which can be easily obtained in this context. However, this limits the search to local minima, which are extremely numerous in such problems, and therefore it is likely each run of the optimization will converge to a different solution.

We first present the barrier implementation, the physical assumptions and the objective function to minimize. Then the expression of the sensitivity with respect to nodes coordinates, based on the shape derivative concept and the adjoint state approach is derived. Finally, the gradient information is used in a classical optimization method to generate new shape-optimized barriers starting from different initial geometries.

2. BARRIER IMPLEMENTATION AND MODELING

2.1 Physical assumptions and geometry

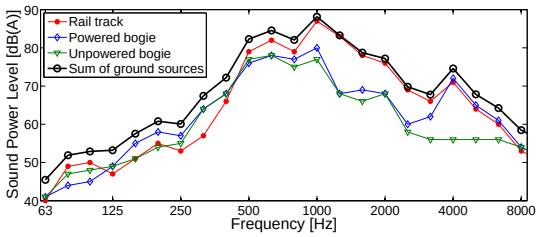

Figure 1 - Comparison of third octave spectra of the different sources identified by Pallas et al. [8] and their incoherent summation.

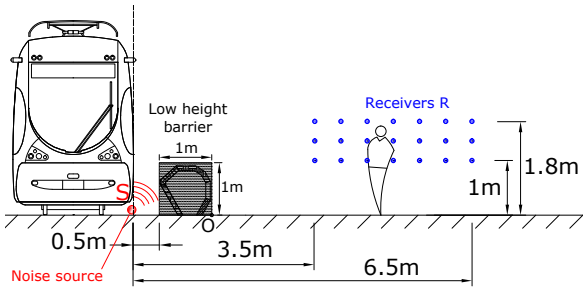

Figure 2 - Geometrical configuration for the implementation of the low-height tramway noise barrier. Dotted line: idealization of the tramway side as a vertical baffle.

The atmosphere is assumed homogeneous with a speed of sound of $c_0 = 343$ m/s. The source is idealized as a infinite line source located on the ground with a spectral content given by the incoherent sum of the rail track and bogie contributions in [8] (see in Figure 1). One can infer that most of the A-weighted acoustic energy is contained in the frequency range 100-2500 Hz, which will be the frequency range of study. It is also assumed that the geometry is invariant along the axis of the track, which makes the problem purely two dimensional. This assumption has been shown [12] to be correct when predicting excess attenuation at single frequencies due to point sources, which is what we will use in the calculation of the broadband attenuation.

The presence of the tramway will cause the sound to bounce on its surface and diffract at the roof edge and at the gap between the carriage and the ground. Those geometrical details could be modeled with the

BEM, but one can also idealize the tramway side as an infinite rigid vertical baffle (see in Figure 2). This is mathematically equivalent to introducing an *image* barrier, symmetrical to the original one with respect to the tramway side surface, which greatly reduces the mesh surface and therefore the computation time. Finally, the ground is modeled as rigid, which represents correctly many urban-like surfaces.

The barrier cross section is assumed to lie in a one meter wide square, half a meter away from the tramway (see in Figure 2). The receiver locations have been chosen to represent a range of possible locations of pedestrian ears: horizontal distance from the bottom-right corner of the barrier between 2 m and 5 m, and height between 1 m and 1.8 m.

2.2 Objective function

The goal of this study is to maximize the insertion loss calculated at the receivers by changing the shape of the barrier. The 2D BEM, implemented in the software MICADO developed at the CSTB by Jean [13], has been used for this purpose. The BEM provides a way to calculate the complex pressure amplitude $p(R, f)$ at each frequency and at each receiver point for an arbitrary geometry. One can then define an average attenuation across all receivers at the frequency f_n:

$$A_n = \left[\frac{\sum_m |p(R_m, f_n)|^2}{\sum_m |p^{\text{in}}(R_m, f_n)|^2} \right]^{\frac{1}{2}} = \frac{P(f_n)}{P^{\text{in}}(f_n)} \tag{1}$$

where $p = p^{\text{in}} + p^{\text{sc}}$ is the total pressure field, p^{in} is the incident field (field without the barrier) and p^{sc} the scattered field. P is an average pressure across the receivers and P^{in} the incident pressure which is a normalizing constant independent of the barrier geometry. Then, a broadband attenuation based on the sound power levels L_w shown in Figure 1 and the attenuations at each frequency is considered. In order to have a somewhat faster evaluation of the objective function (which will be called many times in the optimization) but a good evaluation of the third octave insertion losses, we consider 10 frequencies per third-octave between 100 and 2500 Hz. For each third-octave band, we define an amplitude-like quantity $S = 10^{L_w/10}$, which is assigned to all the frequencies in this third-octave band. The broadband attenuation is then given by:

$$e = \frac{\sum_n S_n A_n^2}{\sum_n S_n} \tag{2}$$

which is similar to the objective function considered by other authors [1, 5]. We would like to minimize the function e, which only depends on the geometry of the barrier (one can also calculate from the objective function a broadband insertion loss in dB(A) defined by $\text{IL} = -10 \log e$). However, it should be pointed out that once the optimization is finished, the broadband and third-octave insertion losses of the barrier will be evaluated more accurately using 20 frequencies per third-octave.

3. DIRECT SCATTERING PROBLEM

In this section, we define the direct scattering problem to solve to calculate the pressure field at the receiver points at each frequency $p(R, f)$, from which one can easily calculate the objective function. The barrier and its image with respect to the vertical baffle are represented by the boundary Γ.

As stated before, the problem is considered purely two-dimensional (the barrier is infinitely extended in one dimension), and is solved in the frequency domain so that the frequency f is fixed and $k = 2\pi f/c_0$ is the wavenumber. The time convention is $e^{-i\omega t}$. Let $G(\mathbf{x}, \mathbf{y})$ be the Green's function of the Helmholtz equation. For a homogeneous atmosphere in presence of a rigid ground, the expression for G is:

$$G(\mathbf{x}, \mathbf{y}) = \frac{i}{4} \left(H_0^{(1)}[k \sqrt{(y_1 - x_1)^2 + (y_2 - x_2)^2}] + H_0^{(1)}[k \sqrt{(y_1 - x_1)^2 + (y_2 + x_2)^2}] \right) \tag{3}$$

where $\mathbf{x} = (x_1, x_2)$ and $\mathbf{y} = (y_1, y_2)$ are two arbitrary points and $H_0^{(1)}$ is the Hankel function of order zero of the first kind.

Let Ω^e and Ω^i be the exterior and interior domains of the barrier, $\mathbf{n}$ the exterior normal of Γ (pointing towards Ω^e). Considering a unit point source at (S), in case of a rigid boundary, the total field p satisfies the problem:

$$\begin{cases} -(\nabla^2 + k^2)\, p = \delta(S, .) \quad \text{in } \Omega^e \\ \dfrac{\partial p}{\partial n} = 0 \quad \text{on } \Gamma \\ \quad + \text{ radiation condition} \end{cases} \tag{4}$$

where $\delta(S,.)$ is the Dirac delta function located at the point (S) and $\partial p/\partial n = \nabla p \cdot \mathbf{n}$ is the normal derivative. One can solve this problem using a boundary element approach, which is based on the integral representation of the field p. Indeed the Kirchhoff-Helmholtz integral theorem states that the total field p at the receiver point (R) is given by:

$$p(R) = p^{\text{in}}(R) + \int_\Gamma \frac{\partial G}{\partial n_y}(R,\mathbf{y}) p_\Gamma(\mathbf{y})\,\mathrm{d}\Gamma(\mathbf{y}) \tag{5}$$

where $p^{\text{in}} = G(S,R)$ is the incident field, $\partial/\partial n_y$ is the normal derivative with respect to $\mathbf{y}$ and p_Γ is the total pressure field on the scatterer Γ, which is here solved numerically with the BEM software MICADO developed by Jean [13].

4. DEFINITION OF THE SHAPE SENSITIVITY

Here we quickly introduce the mathematical concepts used in the calculation of the derivative of the objective function with respect to changes in the shape of the barrier. This section is not meant to be completely rigorous from a mathematical standpoint. For a more rigorous analysis, one can refer to other works [9, 11].

The concept of shape derivative can be understood as a linear form acting on the set of displacements fields, which we will refer to as *velocity* fields. A velocity field $\boldsymbol{\theta}$ is simply a mapping $\mathbf{x} \mapsto \boldsymbol{\theta}(\mathbf{x})$ in $\mathbb{R}^2$. Let D_θ be the set of bounded sufficiently smooth velocity fields in the 2D plane. Such a velocity field transforms the initial boundary Γ to a new boundary $\Gamma(\boldsymbol{\theta})$. Now, consider a complex functional J depending on the boundary Γ. J is said to be differentiable with respect to the shape Γ if there exists a linear form that we will write $\mathrm{d}J/\mathrm{d}\Gamma$ acting on D_θ such that:

$$(\forall \boldsymbol{\theta} \in D_\theta) \quad J(\Gamma(\boldsymbol{\theta})) = J(\Gamma) + \frac{\mathrm{d}J}{\mathrm{d}\Gamma} \cdot \boldsymbol{\theta} + o(\,\|\boldsymbol{\theta}\|_\infty\,) \tag{6}$$

where the dot notation refers to the duality product between D_θ and its dual. For instance, the shape derivatives of simple surface integral is given by [9–11]:

$$F(\Gamma) = \int_{\Omega^e} f\,\mathrm{d}\Omega \qquad \Rightarrow \qquad \frac{\mathrm{d}F}{\mathrm{d}\Gamma} \cdot \boldsymbol{\theta} = \int_{\Omega^e} \nabla \cdot (f\boldsymbol{\theta})\,\mathrm{d}\Omega = -\int_\Gamma f\theta_n\,\mathrm{d}\Gamma \tag{7}$$

where the divergence theorem has been applied. f is a sufficiently smooth function (or generalized function) defined in Ω^e and $\theta_n = \boldsymbol{\theta} \cdot \mathbf{n}$ is the normal component of the velocity field on Γ. One should point out that the minus sign in equation (7) is due to the fact that the normal has been defined as exterior to Γ (hence pointing towards Ω^e).

5. DERIVATION OF THE SENSITIVITY EXPRESSIONS

To carry on the optimization of the objective function, an iterative method based on the gradient has been chosen. Accurate calculation of the sensitivities (derivatives or gradients) with respect to the shape is therefore necessary. We derive here very simple expressions based on the adjoint state approach, which can then be used in a classical gradient-based optimization algorithm.

5.1 General expressions

First, we derive the expression of the shape sensitivity of the RMS pressure P at a given frequency. Let us recall that the total pressure field p satisfies the scattering problem (4). Let us now consider the weak formulation of this problem, as done by Bonnet [10] and He et al. [11], which will allow an easier derivation of the sensitivity expressions. Again, the mathematical treatment given here is not completely rigorous, since special care should be given to the behaviors of the different fields at infinity. More details on this approach can be found elsewhere [11, 14].

Given any sufficiently smooth and locally integrable function $\hat{q}$ which satisfies the radiation condition, the problem (4) is equivalent to [10]:

$$\forall \hat{q} \quad Q(\Gamma, p, \hat{q}) = 0 \qquad \text{with} \quad Q(\Gamma, \hat{p}, \hat{q}) = \mathrm{Re}\left[-\int_\Omega \boldsymbol{\nabla}\hat{p} \cdot \boldsymbol{\nabla}\hat{q}\,\mathrm{d}\Omega + k^2 \int_\Omega \hat{p}\,\hat{q}\,\mathrm{d}\Omega + \hat{q}(S)\right] \tag{8}$$

We now define the Lagrangian $\mathcal{L} = P + Q$. By definition, for all functions $\hat{q}$ we have $Q(\Gamma, p, \hat{q}) = 0$ and therefore $P(\Gamma, p) = \mathcal{L}(\Gamma, p, \hat{q})$. Since p implicitly depends on Γ as the solution of the problem (4), taking the derivative of this last equation with respect to Γ yields:

$$(\forall \hat{q}) \quad \frac{\mathrm{d}P}{\mathrm{d}\Gamma}(\Gamma, p) = \frac{\partial \mathcal{L}}{\partial \Gamma}(\Gamma, p, \hat{q}) + \frac{\partial \mathcal{L}}{\partial p}(\Gamma, p, \hat{q}) \cdot \frac{\mathrm{d}p}{\mathrm{d}\Gamma} \tag{9}$$

Now, let us define the *adjoint state* q as the solution of the following problem:

$$(\forall \hat{w}) \quad \frac{\partial \mathcal{L}}{\partial p}(\Gamma, p, q) \cdot \hat{w} = 0 \tag{10}$$

Now, since equation (9) is valid for any function $\hat{q}$, especially for $\hat{q} = q$, and using equation (10), we have:

$$\frac{\mathrm{d}P}{\mathrm{d}\Gamma}(\Gamma, p) = \frac{\partial \mathcal{L}}{\partial \Gamma}(\Gamma, p, q) \tag{11}$$

which is an explicit function of the shape Γ, the state p and the adjoint state q.

5.1.1 Adjoint state equation

Using simple derivative properties, one can show that the adjoint state problem (10) is given by [10]:

$$(\forall \hat{w}) \quad \mathrm{Re}\Big[-\int_\Omega \boldsymbol{\nabla} q \cdot \boldsymbol{\nabla} \hat{w}\, \mathrm{d}\Omega + k^2 \int_\Omega q\, \hat{w}\, \mathrm{d}\Omega + \sum_m \frac{p(R_m)^*}{P}\, \hat{w}(R_m)\Big] = 0 \tag{12}$$

which is the weak formulation of the following scattering problem:

$$\begin{cases} -(\nabla^2 + k^2)\, q = \displaystyle\sum_m \frac{p(R_m)^*}{P}\, \delta(R_m, .) \quad \text{in } \Omega \\ \qquad \dfrac{\partial q}{\partial n} = 0 \quad \text{on } \Gamma \\ \qquad\quad + \text{ radiation condition} \end{cases} \tag{13}$$

The solution q of this problem is therefore the field due to the radiation of weighted point sources located at the receivers. This problem can be solved once again with the BEM.

5.1.2 Shape derivative expression

In this section, we give the explicit expression of the shape derivative expression given in equation (11). We therefore consider a velocity field $\boldsymbol{\theta}$ acting in the neighborhood of the boundary Γ, and therefore of zero value at the source location (S) and receivers locations (R_m). Let $\theta_n = \boldsymbol{\theta} \cdot \mathbf{n}$ be the normal trace of the velocity field on Γ. We can then apply equation (7) to the expression of Q recalled in equation (8), which yields:

$$\frac{\partial Q}{\partial \Gamma}(\Gamma, p, q) \cdot \boldsymbol{\theta} = \mathrm{Re} \int_\Gamma \theta_n \Big(\boldsymbol{\nabla} p \cdot \boldsymbol{\nabla} q - k^2\, pq\Big)\, \mathrm{d}\Gamma = \mathrm{Re} \int_\Gamma \theta_n \Big(\frac{\partial p}{\partial \tau}\frac{\partial q}{\partial \tau} - k^2\, pq\Big)\, \mathrm{d}\Gamma \tag{14}$$

where the two rigid boundary conditions satisfied by p and q have been used and $\partial/\partial\tau$ is the tangential derivative along the curve Γ.

Now, recalling that the function P explicitly depends only on the field p at the receiver points (R_m) which are not moved by the velocity field $\boldsymbol{\theta}$, we can conclude that the function P does not explicitly depend on the shape Γ when it is transported by $\boldsymbol{\theta}$, and therefore $(\partial P/\partial\Gamma) \cdot \boldsymbol{\theta} = 0$. Recalling equation (11), and since $\mathcal{L} = P + Q$, we have:

$$\frac{\mathrm{d}P}{\mathrm{d}\Gamma}(\Gamma, p) \cdot \boldsymbol{\theta} = \frac{\partial Q}{\partial \Gamma}(\Gamma, p, q) \cdot \boldsymbol{\theta} = \mathrm{Re} \int_\Gamma \theta_n \Big(\frac{\partial p}{\partial \tau}\frac{\partial q}{\partial \tau} - k^2\, pq\Big)\, \mathrm{d}\Gamma \tag{15}$$

Equation (15) is similar to the expression derived by He et al. [11] and Bonnet [10].

5.2 Derivative with respect to a node coordinate

We can now use the general shape derivative expression given in equation (15) to calculate the derivative of the P with respect to parameters describing the shape of the barrier. In order to be as general as possible, we will here consider the derivative with respect to a node coordinate of a "control mesh". Here the BEM discretized assumption implemented in the software MICADO is implied, which is that the boundary Γ is represented by a set of straight segments. Let $\mathbf{x}^{(i)}$ ($i \in [0 : N]$) be the set of control nodes and $\Gamma_i = [\mathbf{x}^{(i-1)}, \mathbf{x}^{(i)}]$ ($i \in [1 : N]$) be each straight segment defining the curve Γ (see in Figure 3). From this set of control nodes, MICADO generates the calculation mesh based on two criteria: a minimum number of elements per segment, and a minimum number of elements per wavelength. The calculation mesh is therefore usually much finer than the mesh defined by the control nodes.

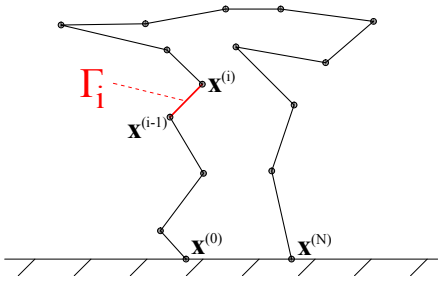

Figure 3 - Representation of a generic barrier based on the control nodes $\mathbf{x}^{(i)}$ and assuming linear interpolation.

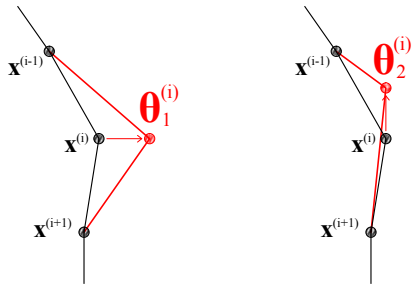

Figure 4 - Definition of the velocity field $\boldsymbol{\theta}_j^{(i)}$, which moves the control node $\mathbf{x}^{(i)}$ along the jth component.

Now, the derivative of P with respect to a change of coordinate of the control node $\mathbf{x}^{(i)} = (x_1^{(i)}, x_2^{(i)})$ can be defined by applying a specific velocity field which moves only this control node along one direction $j = 1, 2$. We therefore define the velocity field $\boldsymbol{\theta}_j^{(i)}$ on the control nodes by:

$$(\forall k \in [0 : N]) \;\; \boldsymbol{\theta}_j^{(i)}\left(\mathbf{x}^{(k)}\right) = \delta_{ik}\, \mathbf{e}_j \tag{16}$$

with δ_{ik} is the Kronecker delta function and $\mathbf{e}_j$ the unit vector in the jth coordinate. Then, on the two segments Γ_i and Γ_{i+1} adjacent to $\mathbf{x}^{(i)}$, the velocity field is linearly interpolated (see in Figure 4). This allows one to define the derivative of P with respect to $x_j^{(i)}$ as:

$$\frac{\mathrm{d}P}{\mathrm{d}x_j^{(i)}} = \frac{\mathrm{d}P}{\mathrm{d}\Gamma} \cdot \boldsymbol{\theta}_j^{(i)} \tag{17}$$

Recalling equation (2), one can then easily write the derivative of the objective function with respect to a node coordinate:

$$\frac{\mathrm{d}e}{\mathrm{d}x_j^{(i)}} = \frac{1}{\sum_n S_n} \sum_n S_n \, \frac{2\, P(f_n)}{P^{\text{in}}(f_n)^2} \, \frac{\mathrm{d}P(f_n)}{\mathrm{d}x_j^{(i)}} \tag{18}$$

We are now able to calculate the gradient of the objective function with respect to the parameters describing the shape. For each frequency, one only needs to know the state and the adjoint state, which is achieved by solving two classical BEM integral equations per frequency. The main advantage of using the adjoint state approach is, once the state and the adjoint state are known, the calculation of each parameter sensitivity is fast (it is an explicit integral), and therefore even if a great number of parameters are used, calculation of the whole gradient is negligible in terms of computation time. Also, the expression of the gradient is simply a post-treatment of the BEM, which implies its calculation does not require coding a new integral equation solver and can be achieved using the results of any commercial BEM software. In this work, the calculation of the states and adjoint states have been achieved using the software MICADO, whereas the calculation of the gradient have been performed in Matlab.

6. OPTIMIZATION ALGORITHM

Thanks to the sensitivity information, one can then use a simple gradient-based optimization algorithm in order to minimize the objective function. Several algorithms exist [15], but it has been chosen to use a very simple *steepest descent* algorithm. As stated before, the shape is described by the set of the $N + 1$ control nodes coordinates, stored in a vector of size $2(N + 1)$ of the form $X = (x_1^{(0)}, ..., x_1^{(N)}, x_2^{(0)}, ..., x_2^{(N)})$. The gradient of the objective function $\nabla e(X)$ is a vector of the same size. At a given iteration k, the shape is updated by:

$$X_{k+1} = \mathbb{P}\Big(X_k - \mu_k \, \nabla e(X_k)\Big) \tag{19}$$

where μ_k is a positive step-size and $\mathbb{P}$ is a projection operator that forces the shape to remain in the constraint box. The step-size is chosen so that the new shape is physical (no loops in the curve) and $e(X_{k+1})$ is sufficiently smaller than $e(X_k)$. More information on this type of algorithm can be found in [9, 15]. The algorithm stops when the variation of e between two iterations is smaller than a tolerance (typically 10^{-4}).

Besides, one should point out that this type of algorithm is limited to local minimum finding. Due to the severe ill-posedness of such shape optimization problems (very numerous local minima), it is very likely that each run of the algorithm will converge to a different solution. Our goal here is therefore to *optimize* a given shape rather than find "the" optimal shape.

7. RESULTS

The algorithm is applied to a few different "starting" geometries, which are shown in Figure 5. The control mesh of each initial geometry is first generated with a maximum distance between two adjacent nodes of 2 cm. Each run of the algorithm stopped after 20 to 40 iterations. Generated optimized shapes are shown in Figure 6. Corresponding broadband insertion losses in the considered frequency range for the initial and optimized shapes are shown in Table 1 and third-octave insertion losses in Figure 7.

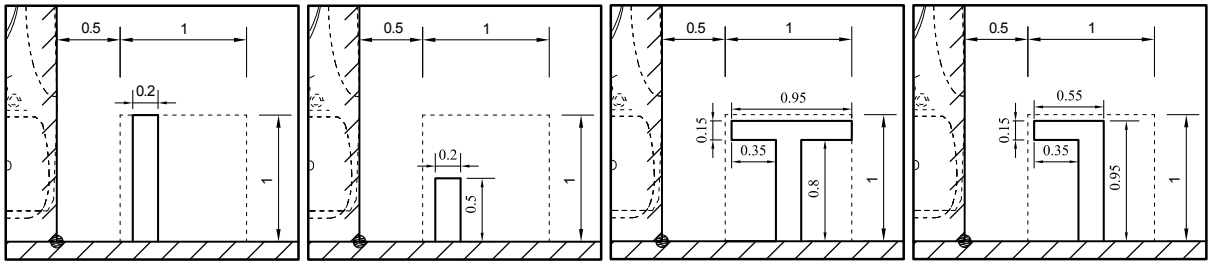

Figure 5 - Definition of the initial geometries. From left to right: straight wall, small wall, T-shape and Gamma-shape. Dimensions are in meters. The dotted line represents the constraint box.

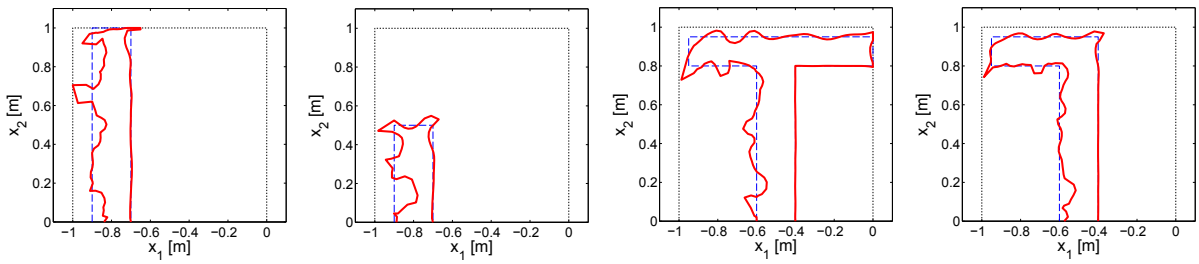

Figure 6 - Initial and optimized geometries for the considered starting geometries defined in Figure 5. Continuous line: optimized geometry - dotted line: initial geometry.

Table 1 - Comparison of broadband insertion losses in dB(A) in the 100-2500 Hz range for the different starting geometries and corresponding optimized geometries.

	Straight wall	Small wall	T-shape	Gamma-shape
Initial	4.2	1.8	5.3	5.9
Optimized	15.2	8.2	11.3	11.1

First of all, one can notice that the shape optimization increased the efficiency significantly in all cases, from + 5 to +11 dB(A). Besides, there seems to be a general trend in the way the shape optimization altered the different geometries: the part of the barrier most exposed to the radiation of the source tends to become more irregular. Especially in the small wall case, instead of increasing the height, the optimization rather made the barrier cross section more irregular, and indeed the broadband efficiency of the optimized small wall is higher than that of the initial straight wall.

Also, from the third-octave insertion losses (see in Figure 7), one can see that all optimized geometries attenuate higher frequencies (above 600 Hz) more efficiently. We believe that this effect is somewhat similar to what has been observed in previous studies [6, 7] when absorbent treatment close to the source is added: efficiencies are higher because multiple reflections phenomena between the barrier and the baffle (tramway side) are somewhat prevented. However, in this case, since the barriers have been assumed rigid, there is no absorption of acoustic energy. The increase of attenuation at higher frequencies might therefore be related to a redirection of the acoustic energy. To have a closer look at this effect, one can compare the intensity map between the initial and optimized geometry, calculated at a frequency where the attenuation is increased, for instance in the straight wall case (see in Figure 8). One can indeed notice that for the optimized geometry, the energy mostly propagates in the x_2 direction, parallel to the vertical baffle, whereas in the initial geometry a significant part of the energy is directed towards the shadow zone. The irregularities therefore seem to force the energy to be redirected before being diffracted, and hence increase the attenuation behind the barrier.

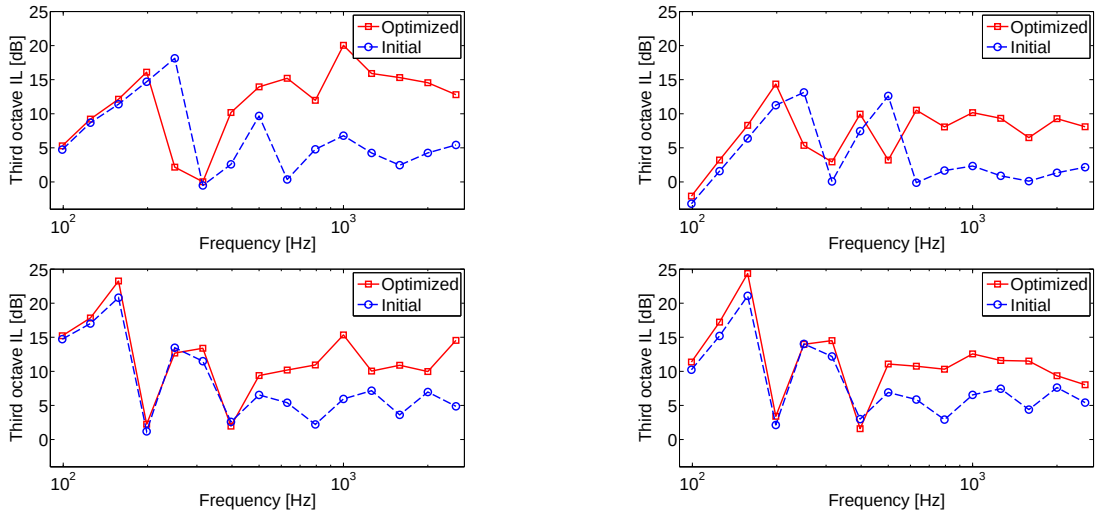

Figure 7 - Comparison of third-octave insertion losses in dB for the different starting geometries and corresponding optimized geometries. Top left: straight wall - top right: small wall - bottom left: T-shape - bottom right: Gamma-shape. Continuous line: optimized geometry - dotted line: initial geometry.

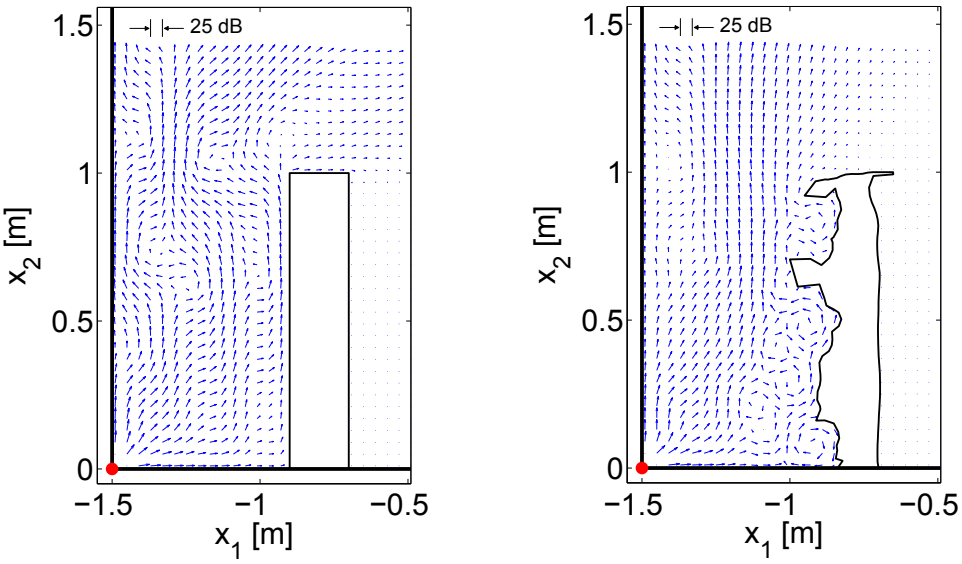

Figure 8 - Comparison of intensity maps at 1000 Hz calculated on a grid of step $h = 4\,\text{cm}$. The intensity vector is calculated as $\mathbf{I} = \text{Re}\,(p^* \mathbf{v})/2$ with $\mathbf{v}$ the particle velocity. Each vector is scaled so that its norm is the norm of the intensity vector $\mathbf{I}$ in dB (length h: reference value (maximum intensity) - length zero: reference minus 25 dB). Left: initial straight wall - right: optimized straight wall.

7.1 Efficiency of a smoothed shape

In order to make sure that the irregularities generated by the shape optimization physically explain the increase of efficiency and are not simply due to numerical artifacts, one can consider smoothed versions of the optimized generated shapes and compare the efficiency of this smoothed shape compared to the original one (see in Figure 9 for the straight wall case). The smoothing is simply based on a low-pass filtering of the nodes coordinates. One can indeed notice that the efficiency is significantly lowered above 600 Hz when the shape is smoothed, which is precisely the range where the attenuation was increased between the initial straight geometry and the optimized irregular geometry. This suggests the presence of the irregularities physically alter the sound field in such a way that the attenuation in the shadow zone is increased.

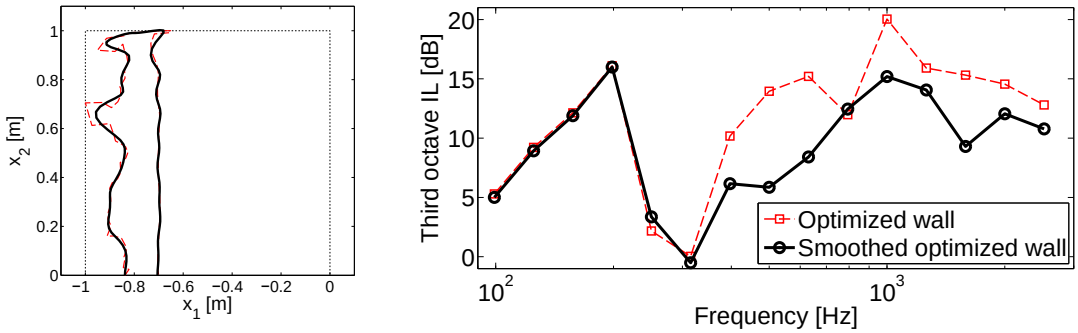

Figure 9 - Comparison of the original and smoothed optimized straight wall geometries. Left: geometry comparison - right: third-octave insertion losses in dB. In both plots, the thin dotted line corresponds to the original optimized geometry and the thick continuous line to the smoothed geometry.

7.2 More advanced numerical modeling

The shape optimization has been carried out under several simplifying assumptions - tramway side represented by a vertical baffle, 2D approximation - in order to keep computation time reasonable since the optimization algorithm evaluates the objective function many times. However, once an optimized design is found, one can use more advanced numerical modeling to evaluate the performance of the generated design in more realistic situations, for instance assuming a more realistic tramway geometry and considering several 3D point sources. This can be done using the so-called 2.5D BEM, developed by Duhamel [12] and implemented in the MICADO software by Jean [16]. For instance, one can replace the coherent line source (which was implicitly assumed in the 2D modeling) by a finite set of incoherent point sources. Here is it assumed the point sources cover a length of 42 m (which is the length of an actual modern tramway), and are placed every 0.5 m. One should also point out that each point source is still assumed omni-directional. Calculations are made up to 1800 Hz only due to the dramatically increased complexity of the model.

Third-octave insertion losses for the initial and optimized straight wall geometries are presented in Figure 10. One can notice that even though the insertion losses are overall reduced in this more realistic situation, the optimized geometry still performs better than the original straight wall above 400 Hz. This induces a benefit on the broadband efficiency in the 100-1800 Hz range of +6 dB(A) (the efficiency being 5.5 dB(A) for the initial wall and 11.5 dB(A) for the optimized geometry). Hence, even with a more realistic geometry and taking into account spatial incoherence of the noise sources, the redirection effect - and the induced benefit - due to the irregularities of the optimized shapes still happens.

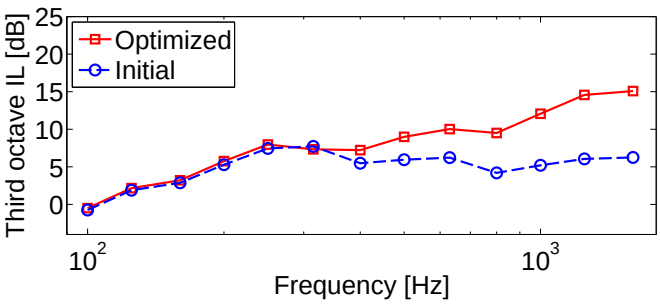

Figure 10 - Comparison of third-octave insertion losses in dB between the initial and optimized straight wall geometry, assuming a realistic tramway cross-section and several incoherent 3D point sources located along the track (covering a length of 42 m).

8. CONCLUSION

The 2D BEM coupled with a simple sensitivity-based optimization algorithm has been used in order to design the shape of a rigid low-height tramway noise barrier. The gradient of the attenuation with respect to each node coordinate can be obtained efficiently using the shape derivative concept and the adjoint state approach, which allows one to vary many parameters without significant increase of the computation time. Also, the sensitivities can be expressed as a post-treatment of the BEM and therefore can be computed from

the output of any commercial BEM software. Besides, several simplifying assumptions can be made to make the calculations faster in the iterative optimization process (2D approximation, rigid ground, tramway side as a vertical baffle).

This method is applied from a few starting geometries (straight walls, T-shape and Gamma-shape barriers). Although each run converged within less than 40 iterations, significant improvement can be achieved, from 6 to 10 dB(A). Generated optimized shapes tend to be very irregular on the side of the barrier directly exposed to the source radiation. Intensity calculations suggest that those irregularities scatter the acoustic energy upwards and therefore prevent some of the energy to be reflected several times and diffracted towards the shadow zone. This effect is observed at mid and high frequencies (above 600 Hz), but not at low frequencies. It has also been observed that smoothing the shape decreases the efficiency, which suggests irregularities are not numerical artifacts, but physically alter the sound field to increase the attenuation in the shadow zone thanks to the redirection effect.

Finally, the generated optimized shape still performs better than a simple shape even when considering a more realistic tramway geometry and source modeling. This suggests that the generated optimized barriers would be more efficient than simple ones in reality. However, one can point out predictions have been done under the assumption of omnidirectional sources, and it is likely that realistic directivity patterns would change the results. Actual *in situ* performance measurements would therefore be necessary to confirm the benefit of such optimized shape barriers.

ACKNOWLEDGMENTS

The authors would like to thank the French Ministry of Ecology, Sustainable Development and Energy (MEDDE) for the financial support of this work.

REFERENCES

[1] M. Baulac, "Optimisation des protections anti-bruit routières de forme complexe (optimization of complex traffic noise barriers)," Ph.D. dissertation, Université du Maine (Le Mans, France, 2006).

[2] M. Baulac, J. Defrance, P. Jean, and F. Minard, "Efficiency of noise protections in urban areas: prediction and scale model measurements," Acta Acust. United Ac., 92, 530–539 (2006).

[3] P. J. Thorsson, "Optimisation of low-height noise barriers using the equivalent sources method," Acta Acust., 86, 811–820 (2000).

[4] P. J. Thorsson, "Combined effects of admittance optimisation on both barrier and ground," Appl. Acoust., 64, 693–711 (2003).

[5] F. Koussa, "Evaluation de la performance acoustique des protections antibruit innovantes utilisant des moyens naturels : application aux transports terrestres (evaluation of the acoustic efficiency of innovative noise barriers using natural means: application to ground transportation systems)," Ph.D. dissertation, Ecole Centrale de Lyon (Lyon, France, 2012).

[6] A. Jolibois, D. Duhamel, V. W. Sparrow, J. Defrance, and P. Jean, "Scattering by a cylinder covered with an arbitrary distribution of impedance and application to the optimization of a tramway noise abatement system," J. Sound Vib., 331, 5597–5622 (2012).

[7] A. Jolibois, D. Duhamel, V. W. Sparrow, J. Defrance, and P. Jean, "Application of admittance optimization to the design of a low-height tramway noise barrier," Proc. INTER-NOISE 2012, (2012).

[8] M. A. Pallas, J. Lelong, and R. Chatagnon, "Characterization of tram noise emission and contribution of the noise sources," Appl. Acoust., 72, 437–450 (2011).

[9] G. Allaire, *Conception optimale des structures (Optimal design of structures)* (Springer, 2007).

[10] M. Bonnet, "BIE and material differentiation applied to the formulation of obstacle inverse problems," Eng. Anal. Bound. Elem., 15, 121–136 (1995).

[11] L. He, S. Kindermann, and M. Sini, "Reconstruction of shapes and impedance functions using few far-field measurements," J. Comput. Phys., 228, 717–730 (2009).

[12] D. Duhamel, "Efficient calculation of the three-dimensional sound pressure field around a noise barrier," J. Sound Vib., 197(5), 547–571 (1996).

[13] P. Jean, "A variational approach for the study of outdoor sound propagation and application to railway noise," J. Sound Vib., 212(2), 275–294 (1998).

[14] I. Terrasse and T. Abboud, *Modélisation des phénomènes de propagation d'ondes (Modeling of wave propagation phenomena)* (Ecole Polytechnique, 2007).

[15] J. Nocedal and S. J. Wright, *Numerical optimization* (Springer, 2006).

[16] P. Jean, J. Defrance, and Y. Gabillet, "The importance of source type in the assessment of noise barriers," J. Sound Vib., 226(2), 201–216 (1999).